Electronic Supplementary Material (ESI) for Chemical Communications.

Supporting Information

Porous Li-MOF as Solid-State Electrolyte: Exploration of Lithium Ion Conductivity through Bio-inspired Ionic Channels

Karabi Nath,[†] Abdulla Bin Rahaman,[‡] Rajib Moi,[†] Kartik Maity,[†] and Kumar Biradha[†]*

[†]Department of Chemistry, Indian Institute of Technology, Kharagpur-721302, India

*Fax: 91-3222-282252; Tel: 91-3222-283346 *E-mail: kbiradha@chem.iitkgp.ernet.in*

[‡]Department of Physics, Indian Institute of Technology, Kharagpur-721302, India

Table of Contents:

General Aspects:

All chemicals including anthracene, 1,2,4,5-tetramethyl benzene, paraformaldehyde, and dimethyl-5-hydroxyisophthalate were obtained from Sigma-Aldrich. All other solvents including glacial acetic acid and HBr were freshly distilled prior to use. Fourier transform IR (FTIR) spectra were recorded with a Perkin-Elmer instrument. Thermogravimetric analysis (TGA) data were recorded under nitrogen atmosphere at a heating rate of 5ºC/min with a Perkin-Elmer instrument, Pyris Diamond TG/DTA. Powder X-ray diffraction (PXRD) data were recorded with a BRUKER-AXS-D8-ADVANCE diffractometer at room temperature. ^{1}H NMR (200/400/600 MHz) spectra were recorded on a BRUKER-AC 200/400/600 MHz. spectrometer. Melting points were recorded using a Fisher Scientific melting point apparatus cat. No. 12-144-1. The surface morphology of the samples were characterized by using a field emission scanning electron microscope (ZEISS EVO 60 with oxford EDS detector).

Section S1: Synthesis of Carboxylate Ligands and Characterizations

Synthesis of **H_4TMCA**:-

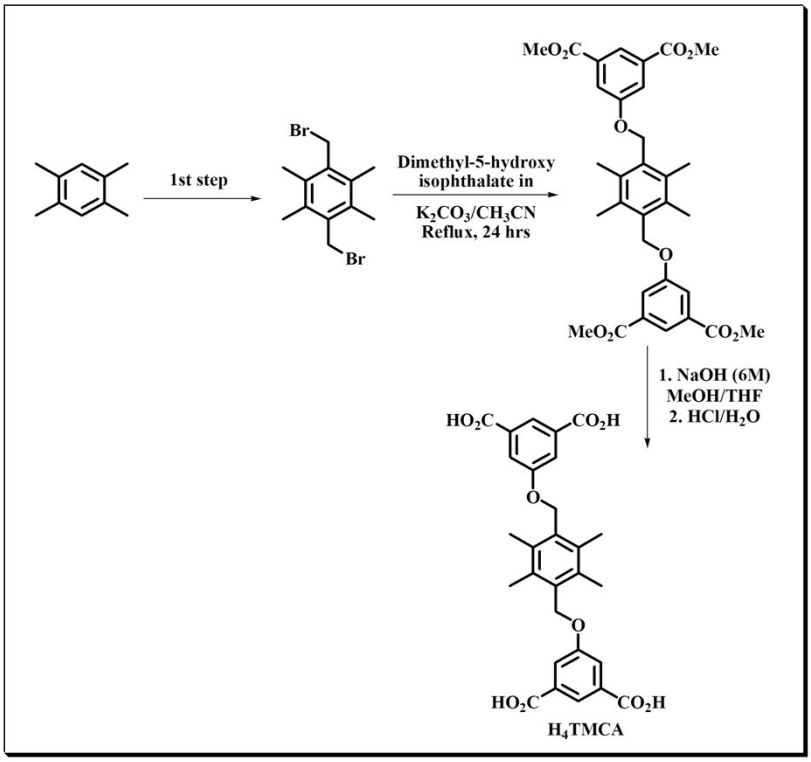

Preparation of the tetramethyl-ester: In the first step, 1,4-Bis(bromomethyl)-2,3,5,6-tetramethyl benzene was prepared from 1,2,4,5-tetramethyl benzene following a reported literature procedure with slight modifications.[S1] In the next step, a mixture of dimethyl 5-hydroxy isophthalate (919 mg, 4.38 mmol) and K_2CO_3 (908 mg, 6.57 mmol) was taken in a two neck RB in presence of dry acetonitrile solvent and heated for at least half an hour at 80^{o}C. 1,4-Bis(bromomethyl)-2,3,5,6-tetramethyl benzene (700 mg, 2.19 mmol) was subsequently added into this reaction mixture and the entire solution was refluxed for 24 hrs at 80^{o}C. After the completion of the reaction, it was quenched by adding water leading to the formation of a white curdy precipitate. The precipitate was filtered and washed thoroughly with water and then dried under vacuum. The resulting tetramethyl-ester obtained here was used in the next step for hydrolysis. Yield = 85%.

Hydrolysis of the ester to obtain H_4TMCA: The tetramethyl-ester (800 mg, 1.38 mmol) was taken in a RB and 100 ml of 6M NaOH solution in MeOH/THF solvent mixture was added to it. The resulting solution mixture was then stirred at room temperature for about 48 hrs. After this, the solution was worked up with aqueous HCl, leading to the formation of the tetra-acid (**H_4TMCA**) as a white precipitate. The resulting precipitate was washed thoroughly with water for several times and dried under vacuum. The product was further characterized by ^{1}H NMR and ^{13}C NMR spectroscopy.

Yield = 75%, m.p = 237-240^{o}C.

Synthesis of **H_4AOIA**: The anthracene based tetracarboxylic acid (**H_4AOIA**) was prepared in the similar way, starting from 9,10-Bis-bromomethyl anthracene following a previously reported procedure.[S2]

^{1}H NMR Spectrum of H_4TMCA in d_6-DMSO:-

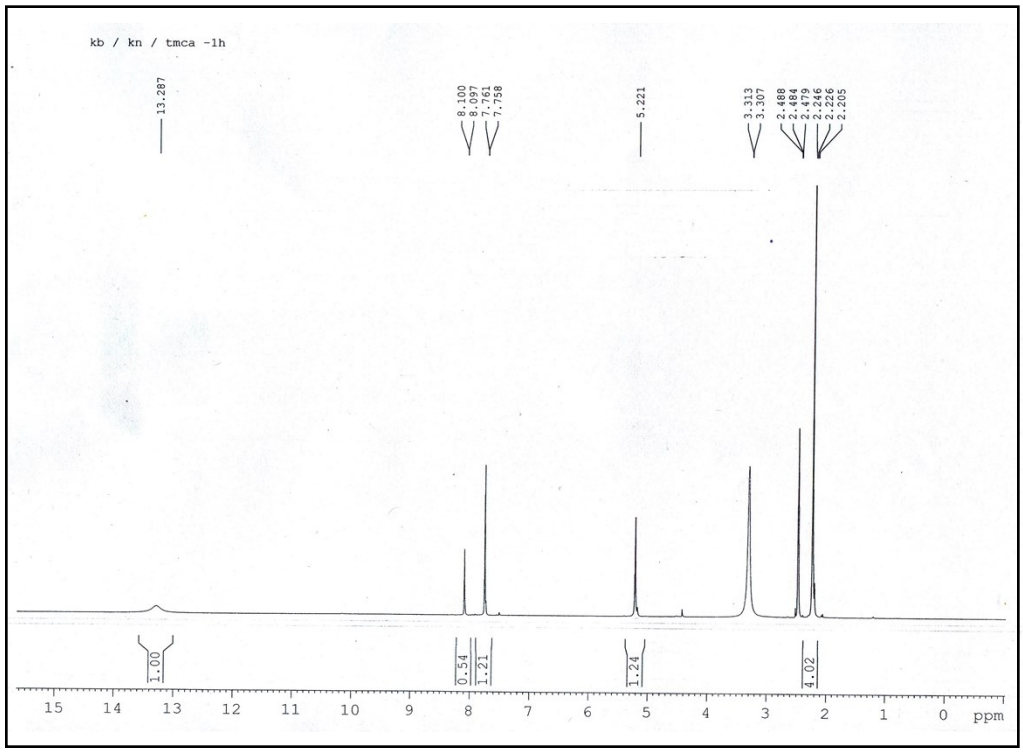

^{13}C-NMR Spectrum of H_4TMCA in d_6-DMSO:-

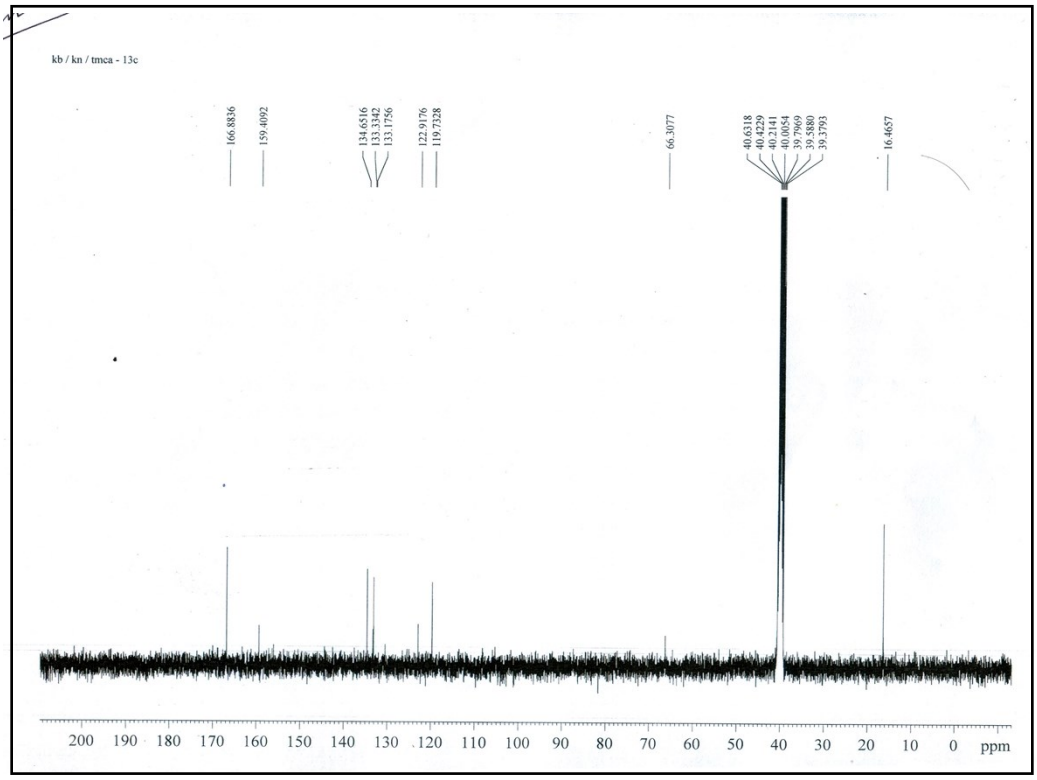

Section S2: Preparation of Li-MOF based solid electrolytes

Synthesis of **Li-AOIA**: The as-synthesized ligand **H_4AOIA** (28.3 mg, 0.05 mmol) was mixed with Li(NO_3) (7 mg, 0.1 mmol) in presence of 4 ml DMF/ethanol solvent mixture (3:1). The resulting solution was taken in a 15 ml Pyrex tube and heated in an oven at 80^{o}C for 24 hrs under solvothermal conditions. Upon cooling down to room temperature, it resulted in the formation of long needle shaped yellow colored crystals, suitable for SXRD analysis. Yield: ~75%.

Synthesis of **Li-AOIA@X** (X = Cl^-, Br^-, I^-, BF_4^- and NO_3^-): **Li-AOIA** crystals were filtered and washed thoroughly with ethanol. It was then immersed in acetone for 7 days during which the crystals were exchanged with fresh acetone for several times. The acetone exchanged crystals were then activated at 80^{o}C for 12 hrs to generate the desolvated framework of **Li-AOIA**. The desolvated **Li-AOIA** powder (50 mg) were then soaked into a 1M LiX)/ethanolic solution (10 ml) for about 24 hrs. The resulting material was then washed thoroughly with ethanol, vacuum filtered and air dried to obtain the free flowing powder of **Li-AOIA@X.** ICP-AES analysis indicated the percentage uptake of Li-content in each of these materials.

Synthesis of **Li-TMCA**: The as-synthesized ligand **H_4TMCA** (26.1 mg, 0.05 mmol) was mixed with Li(NO_3) (7 mg, 0.1 mmol) in presence of 4 ml DMF/ethanol solvent mixture (3:1). The resulting solution was taken in a 15 ml Pyrex tube and heated in an oven at 80^{o}C for 24 hrs under solvothermal conditions. Upon cooling down to room temperature, it resulted in the formation of small white plate shaped crystals, suitable for SXRD analysis. Yield: ~80%.

Synthesis of **Li-TMCA@X** (X = BF_4^- and NO_3^-): The synthesis was performed in the similar procedure as of **Li-AOIA@X**. Further, ICP-AES analysis indicated the amount of increased Li-content in **Li-TMCA@BF_4** and **Li-TMCA@NO_3**.

Section S3: Single Crystal Structure Analysis

Crystal Structure Determination:

The single crystal data was collected on a Bruker-APEX-II CCD X-ray diffractometer that uses graphite monochromated Mo Kα radiation (λ = 0.71073 Å) at low temperature (100 K) by the. hemisphere method. The structure was solved by direct methods and refined by least-squares methods on F^2 using SHELXL-2014.[S3] Non-hydrogen atoms were refined anisotropically, and hydrogen atoms were fixed at calculated positions and refined using a riding model. The H atoms attached to the O atom or N atoms are located wherever possible and refined using the riding model.

Table S1: Crystallographic parameters for Li-AOIA and Li-TMCA

Formula	$C_{36}H_{30}Li_2N_5O_{13}$	$C_{34}H_{38}Li_2N_2O_{12}$
Mol.Wt.	754.53	680.54
T (K)	100(2)	100(2)
System	Monoclinic	Monoclinic
Space group	C2/c	C2/c
a (Å)	23.699(3)	21.900(3)
b (Å)	16.6746(2)	16.990(2)
c (Å)	10.1581(1)	9.436(2)
α (°)	90.00	90.00
β (°)	101.153(3)	109.177(5)
γ (°)	90.00	90.00
V (A^3)	3938.3(8)	3316(8)
Z	4	4
D(g/cm^3)	1.273	1.363
R_1 [I > 2σ(I)]	0.0691	0.0679
wR_2 (on F^2, all data)	0.2168	0.2294

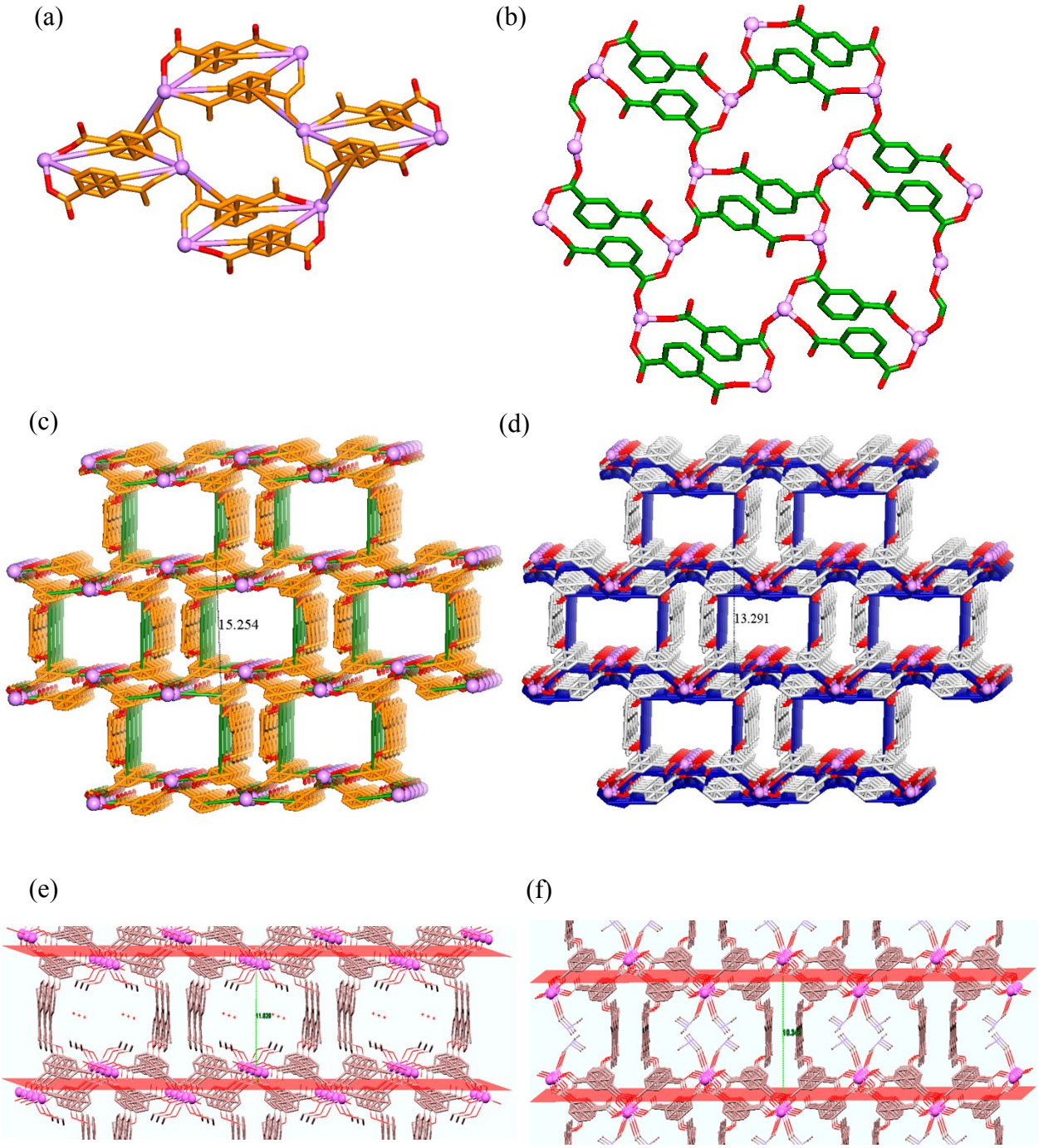

Fig. S1 (a) Three connected node formed by both Li(I) and isophthalate moiety in the Li-MOFs; (b) 2D-double layer formed by the isophthalate connectivities; (c) & (d) Topological representation of the 3D-porous framework in **Li-AOIA** and **Li-TMCA** respectively; (e) & (f) interlayer separations in **Li-AOIA** and **Li-TMCA** respectively.

Section S4: Powder X-ray diffraction Patterns

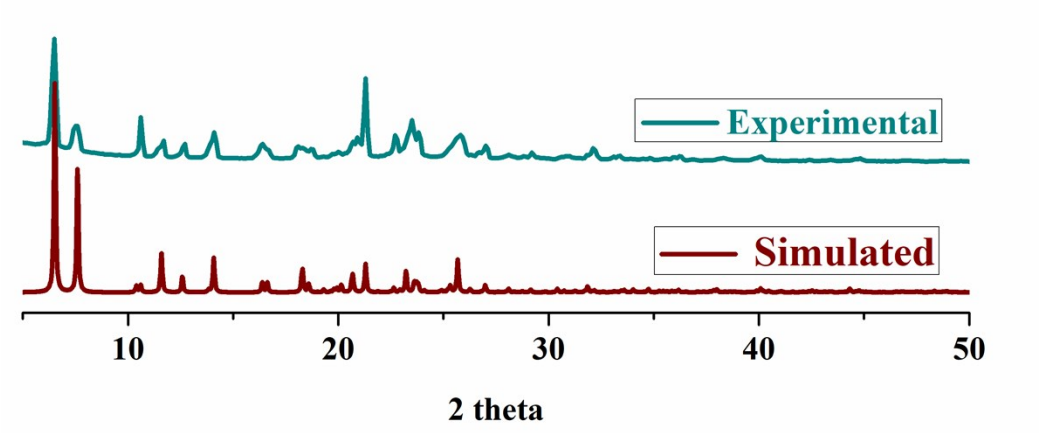

Fig. S2 Comparison of experimental and simulated powder patterns of **Li-AOIA**

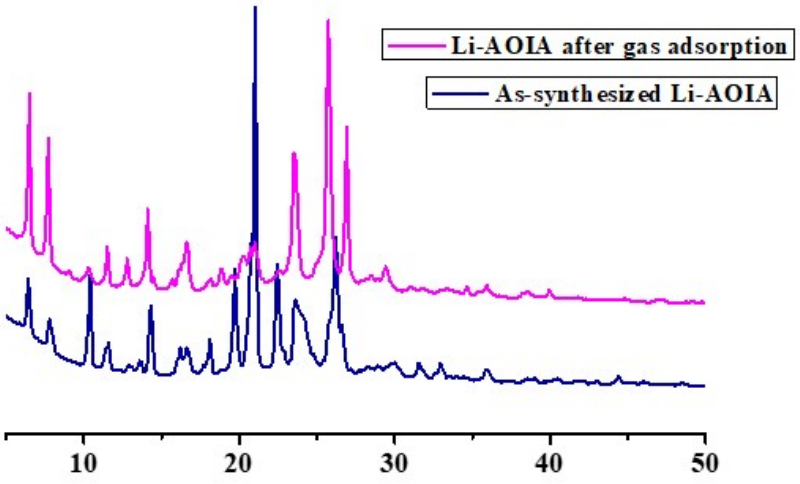

Fig. S3 Experimental powder patterns of **Li-AOIA** after gas adsorption analysis

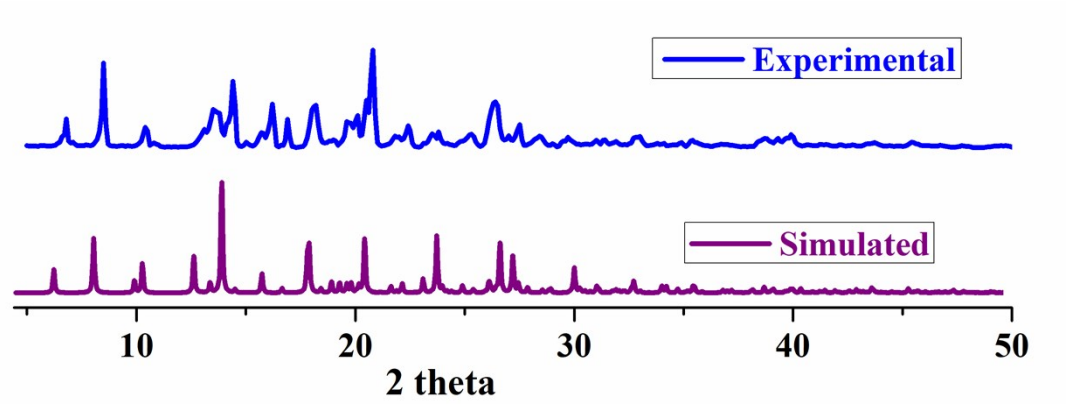

Fig. S4 Comparison of experimental and simulated powder patterns of **Li-TMCA**

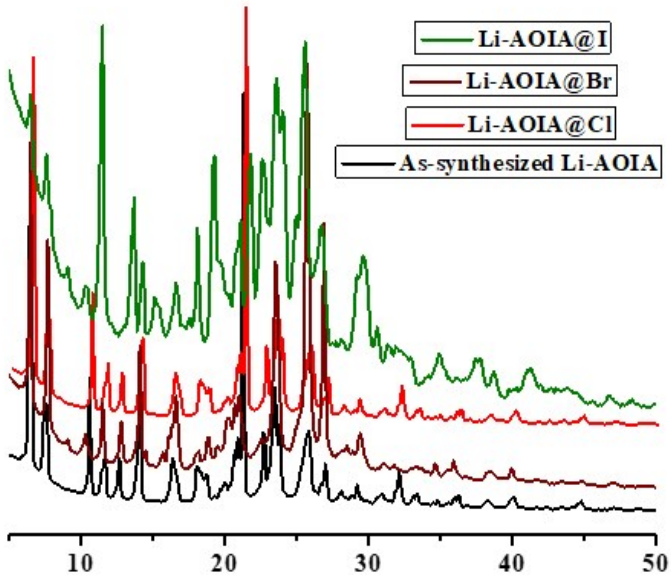

Fig. S5 Experimental powder patterns of the halide doped **Li-AOIA** materials.

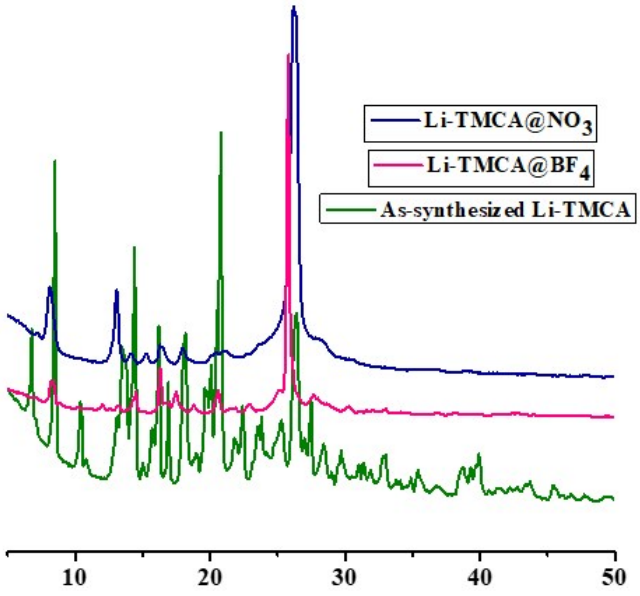

Fig. S6 Experimental powder patterns of **Li-TMCA@NO_3** and **Li-TMCA@BF_4.** Notice the difference in their powder patterns from that of **Li-TMCA**.

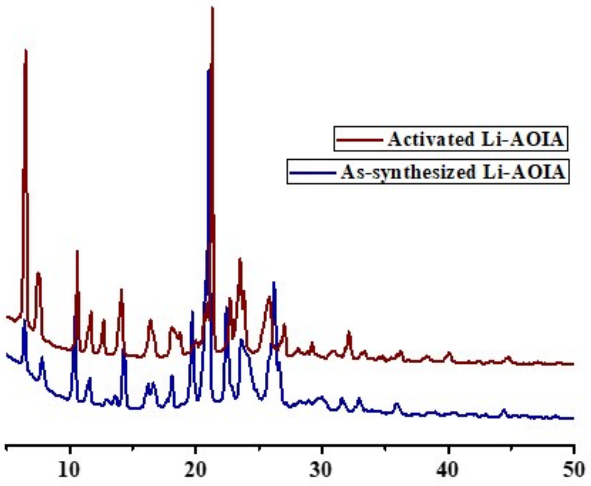

Fig. S7 Comparison of experimental powder patterns of activated and as-synthesized **Li-AOIA**.

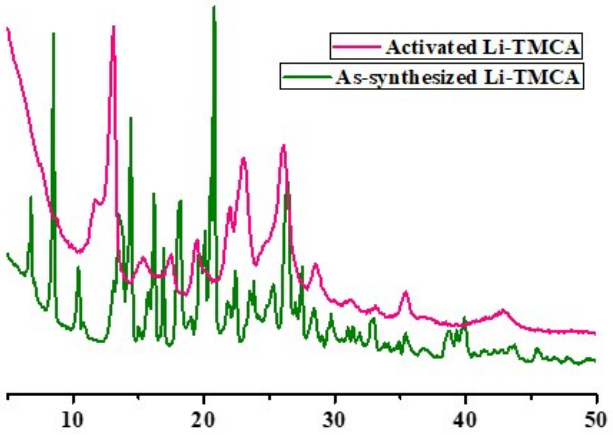

Fig. S8 Comparison of experimental powder patterns of activated and as-synthesized **Li-TMCA**.

Section S5: Thermogravimetric Analysis (TGA) of Li-MOF

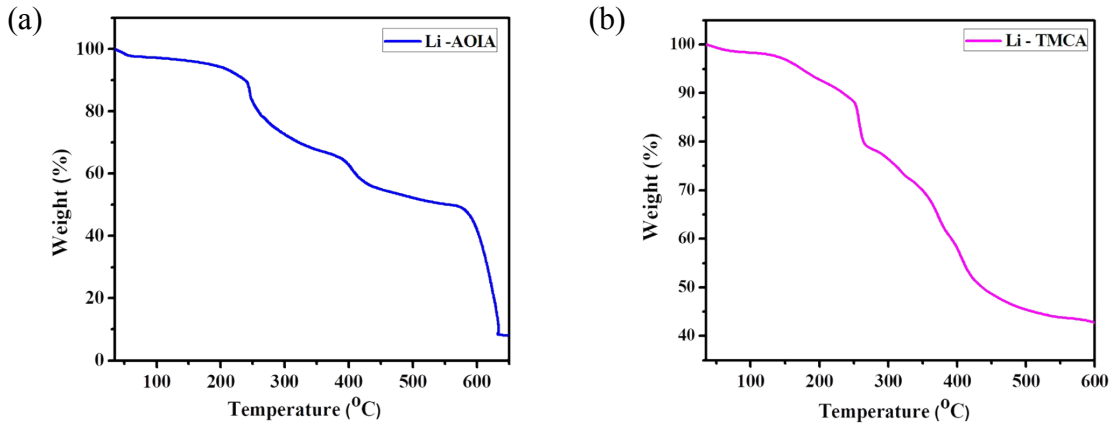

Fig. S9 Determination of thermal stability of **Li-AOIA and Li-TMCA.**

Section S6: FTIR Spectroscopic Analysis

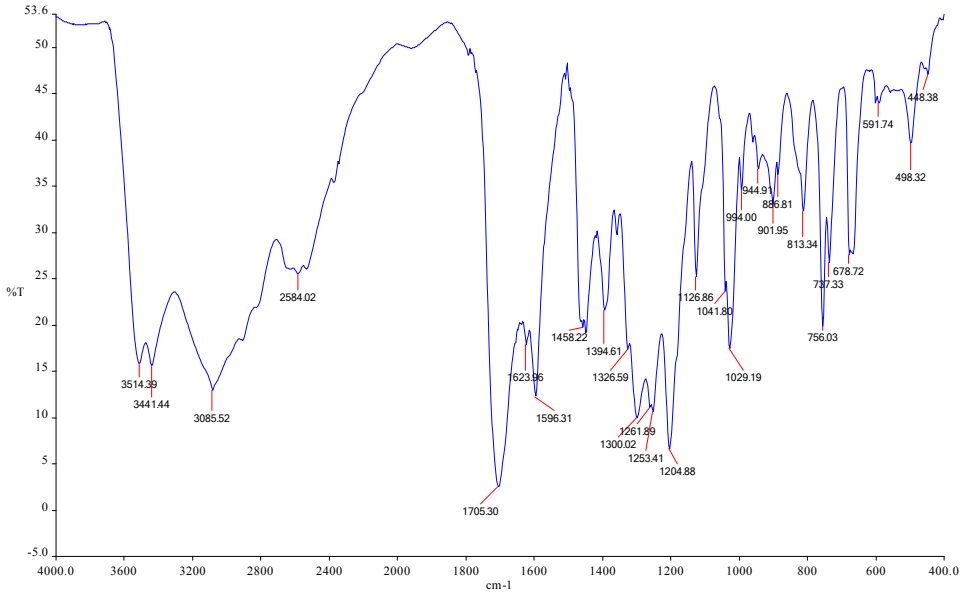

Fig. S10 FTIR spectra of **H_4AOIA**.

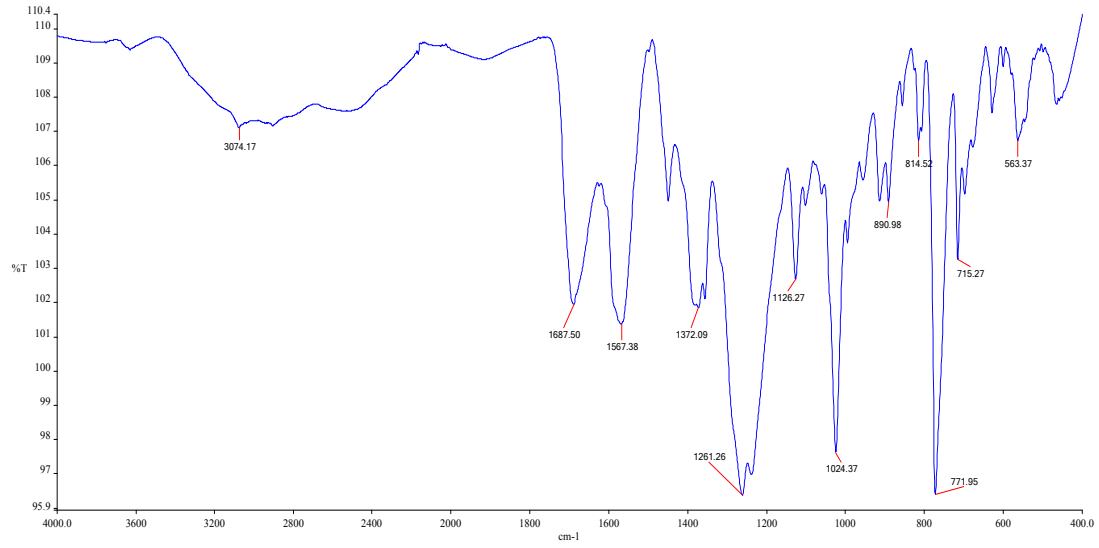

Fig. S11 FTIR spectra of **Li-AOIA**.

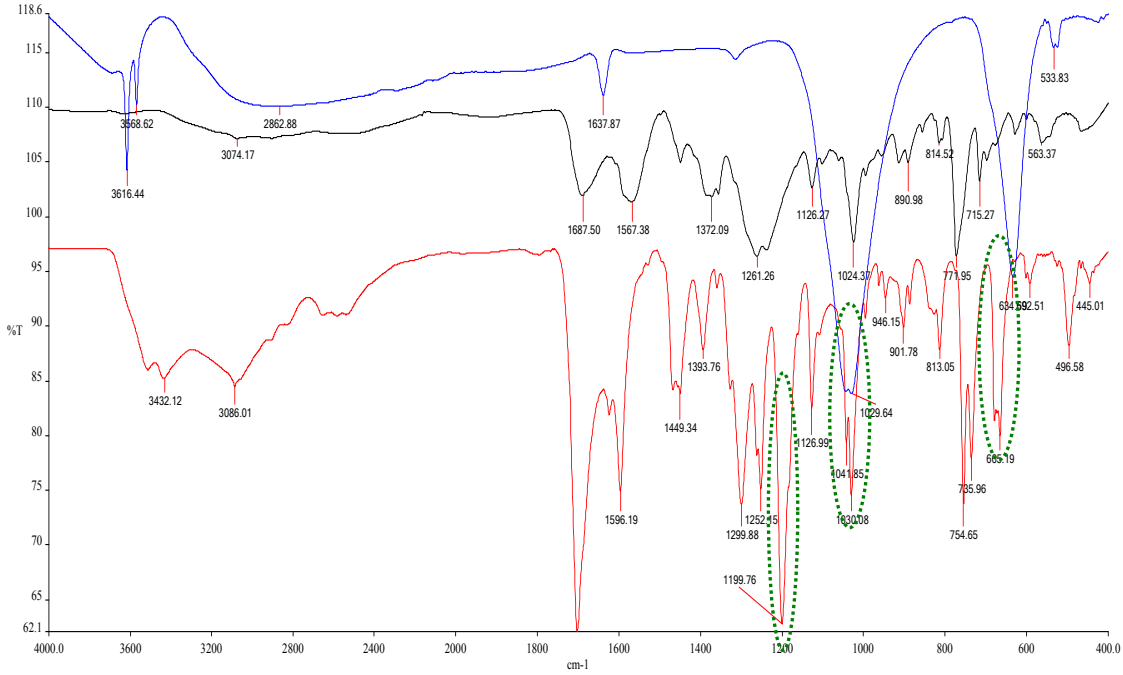

Fig. S12 FTIR spectra of **Li-AOIA** (black), $LiBF_4$ salt (blue) and **Li-AOIA@BF_4** (red). Emergence of new peaks at a higher stretching frequency with strong intensities indicates the coordination of the respective counter-anion BF_4 to the open metal sites. This also corresponds to the asymmetric stretching modes generated due to the coordination, disrupting the symmetric vibrations (T_d symmetry is reduced to C_{3v}).

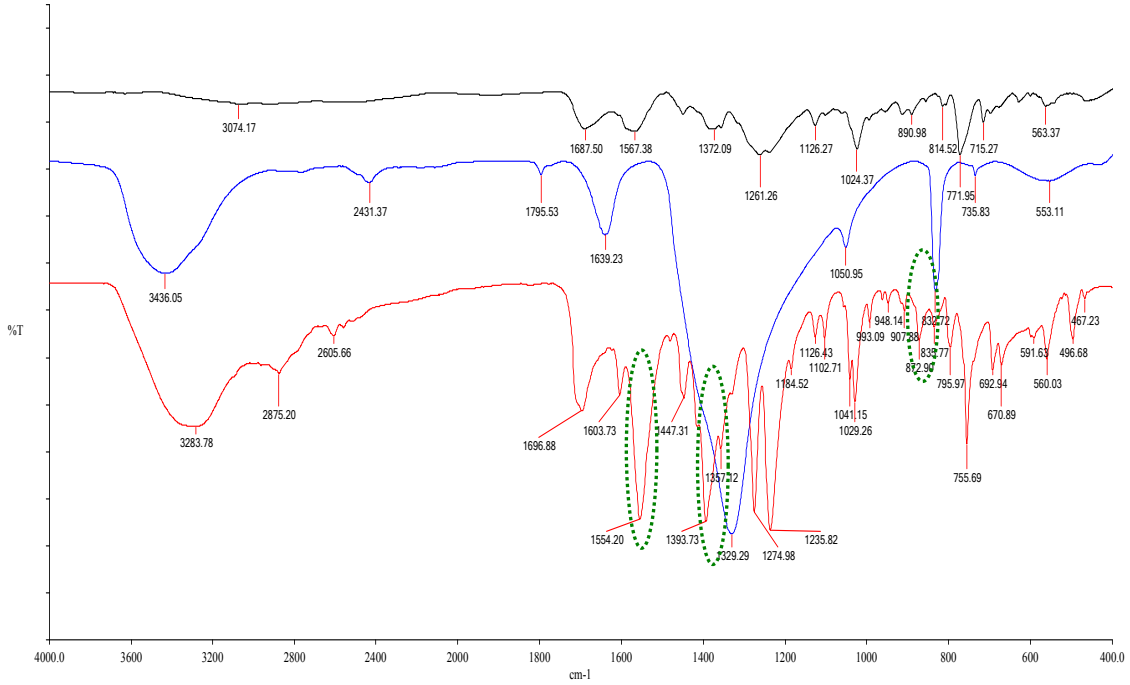

Fig. S13 FTIR spectra of **Li-AOIA** (black), $LiNO_3$ salt (blue) and **Li-AOIA@NO_3** (red). Emergence of new peaks at a higher stretching frequency with strong intensities indicates the coordination of the respective counter-anion NO_3 to the open metal sites. This also corresponds to the asymmetric stretching modes generated due to the coordination, disrupting the symmetric vibrations (D_{3h} symmetry is reduced to C_{2v}).

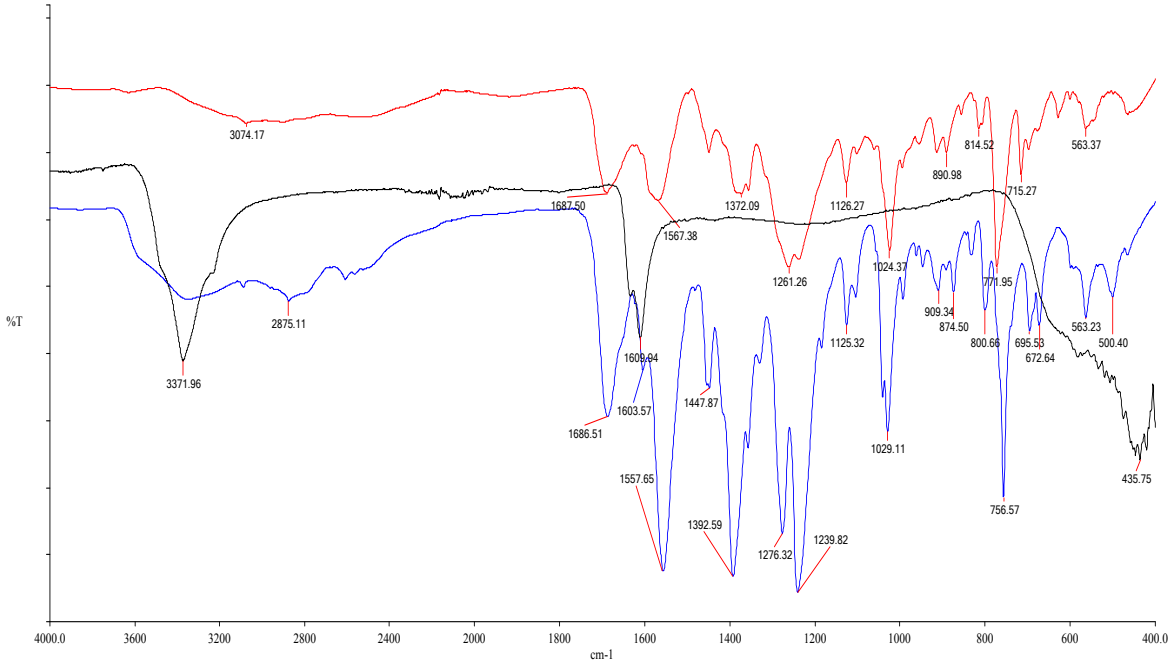

Fig. S14 FTIR spectra of **Li-AOIA** (red), LiBr salt (black) and **Li-AOIA@Br** (blue).

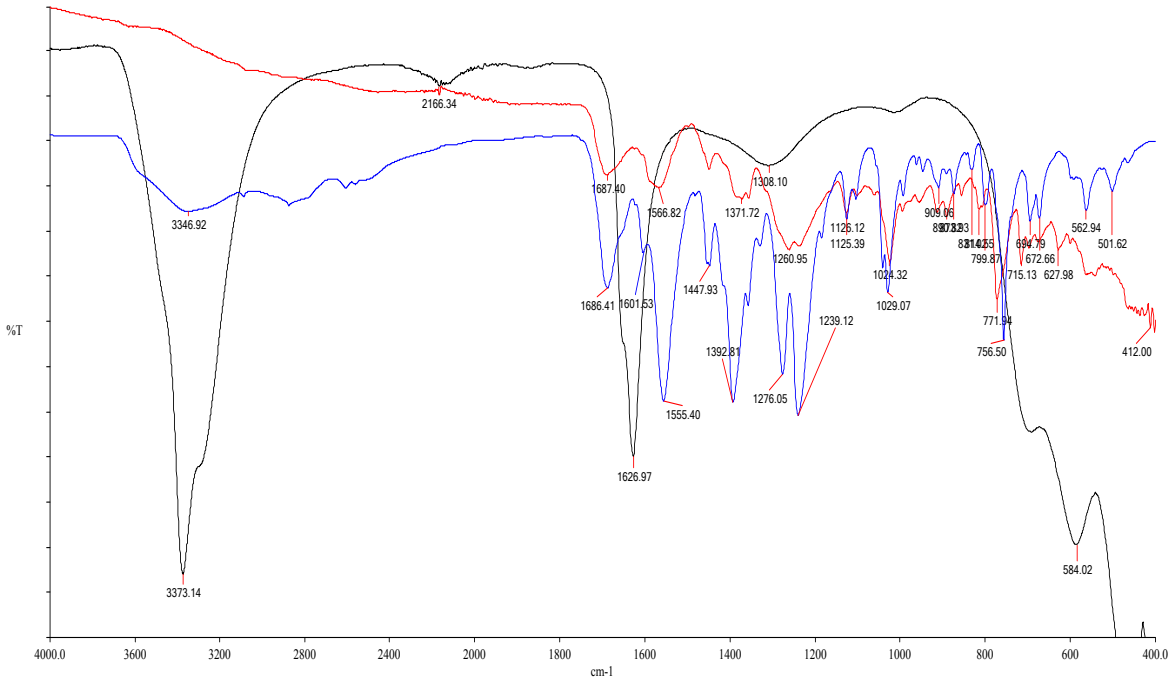

Fig. S15 FTIR spectra of **Li-AOIA** (red), LiCl salt (black) and **Li-AOIA@Cl** (blue).

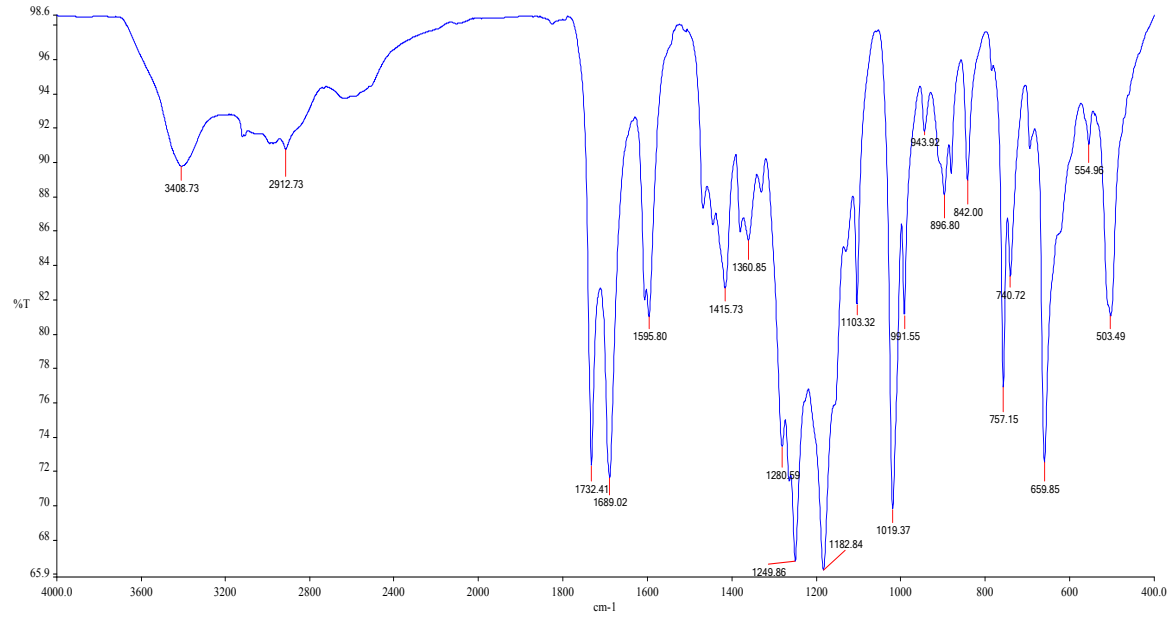

Fig. S16 FTIR spectra of **H_4TMCA**

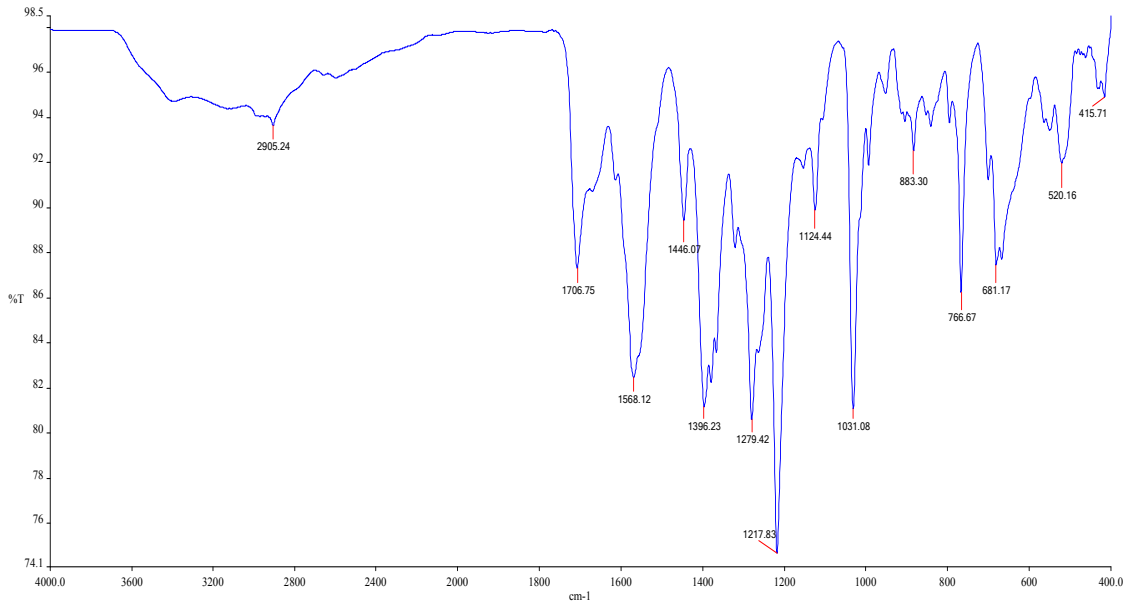

Fig. S17 FTIR spectra of **Li-TMCA**

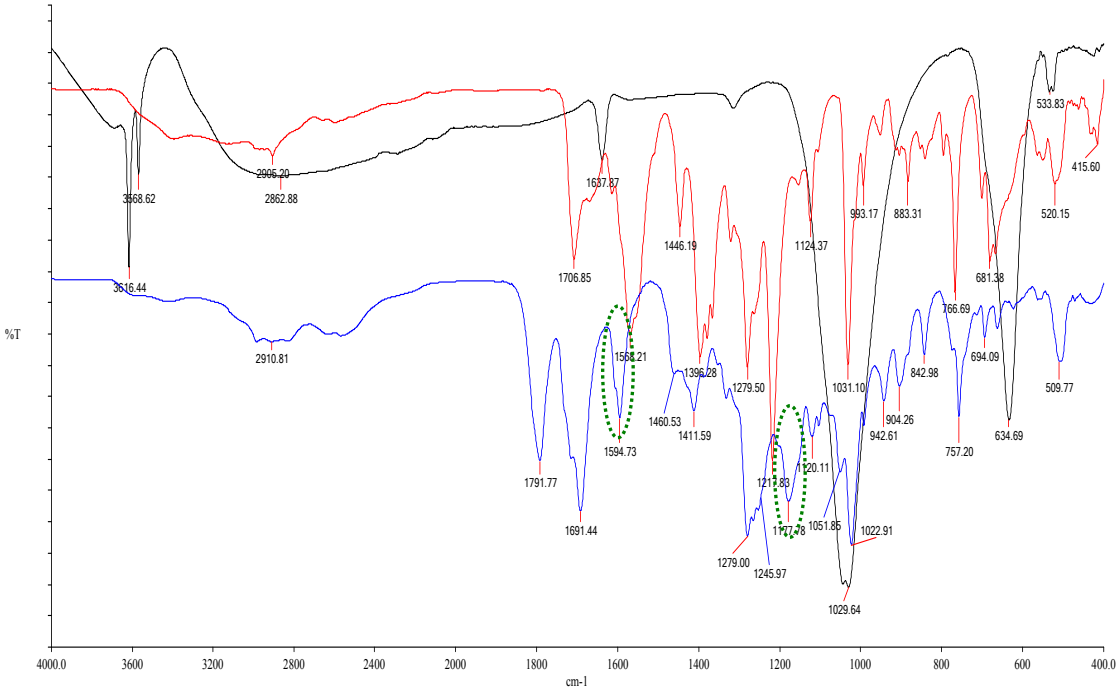

Fig. S18 FTIR spectra of **Li-TMCA** (red), $LiBF_4$ salt (black) and **Li-TMCA@BF_4** (blue). Emergence of new peaks at higher stretching frequencies indicates coordination of BF_4^- anion with the open metal sites.

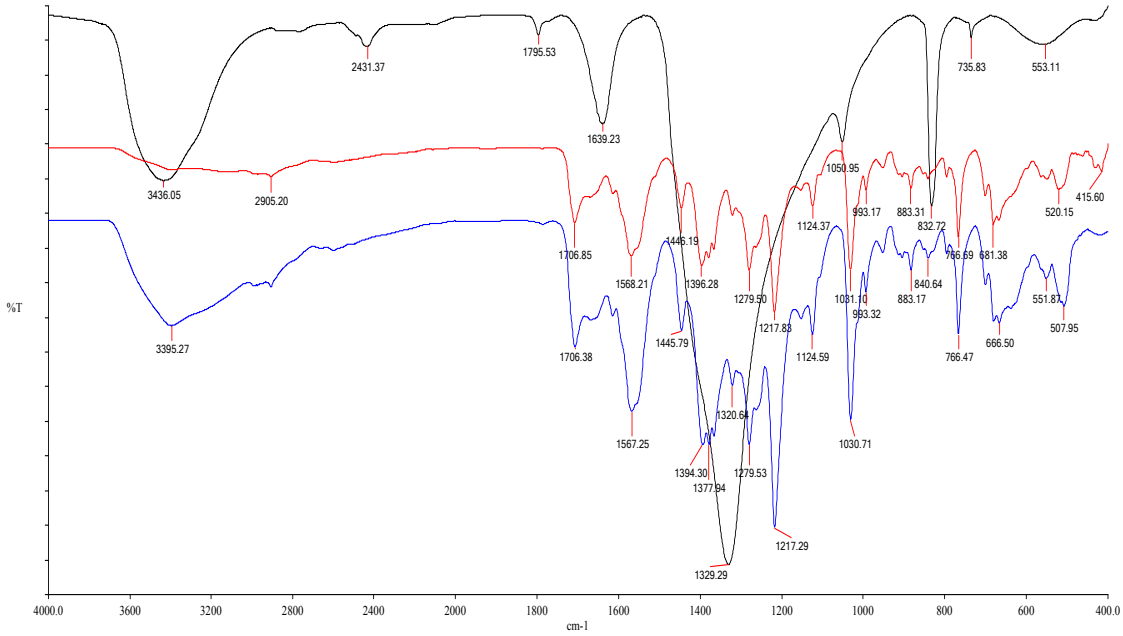

Fig. S19 FTIR spectra of **Li-TMCA** (red), $LiNO_3$ salt (black) and **Li-TMCA@NO_3** (blue). The spectra for **Li-TMCA** and **Li-TMCA@NO_3** are almost similar which indicates weaker interactions of NO_3^- anions with the open metallic sites in **Li-TMCA@NO_3.**

Section S7: ^{1}H NMR spectra of salt treated Li-MOF samples

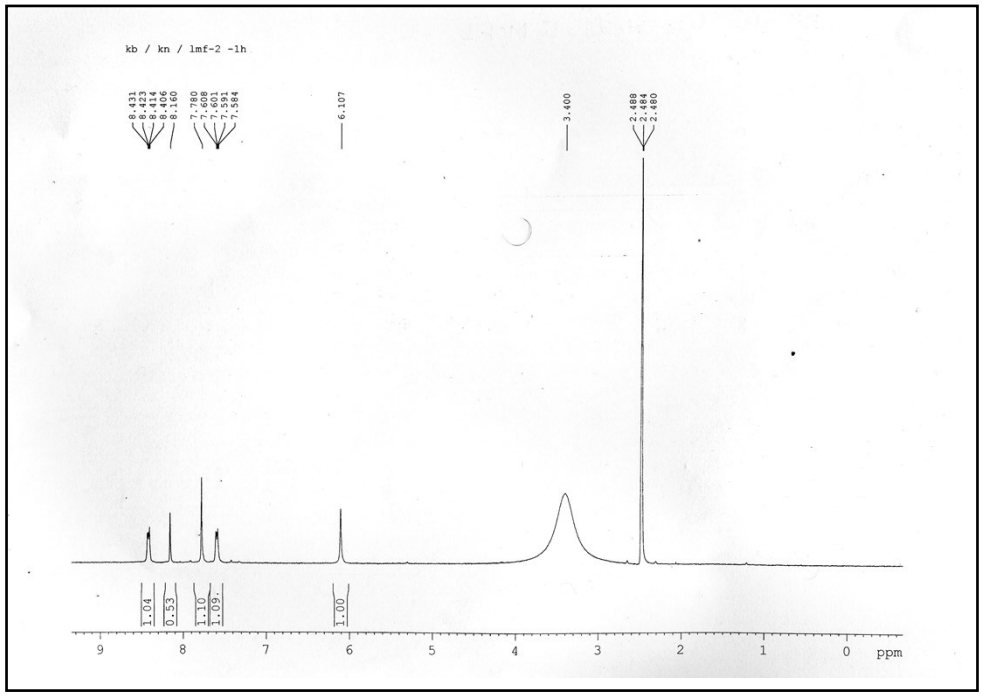

Fig. S20 ^{1}H NMR spectrum of digested **Li-AOIA@NO_3**.

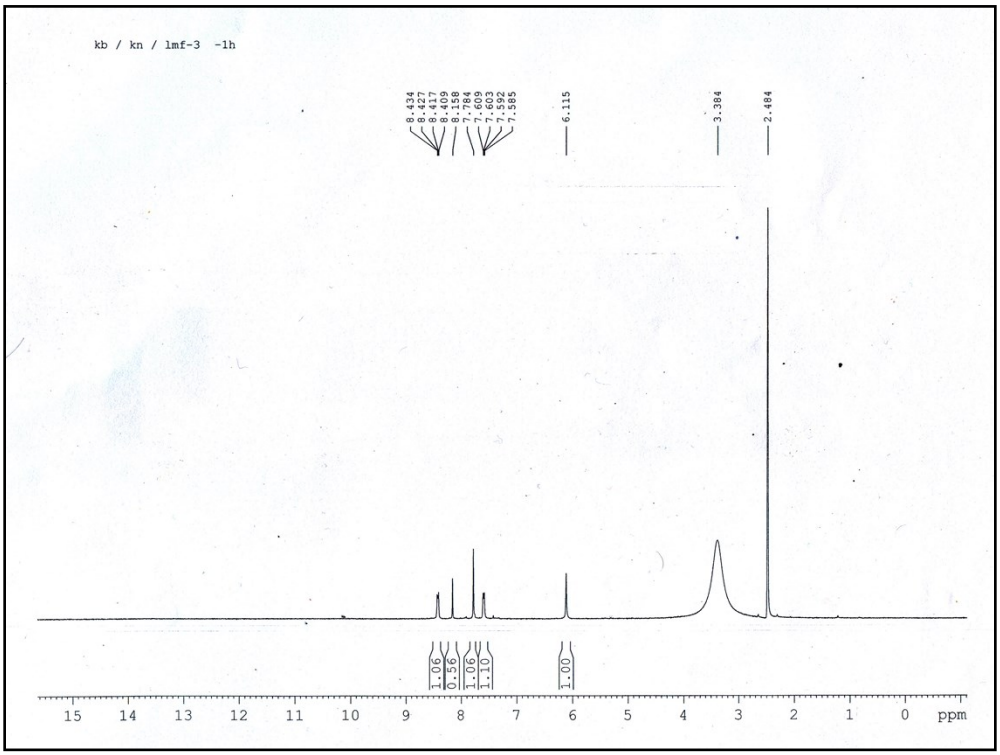

Fig. S21 [1]H NMR spectrum of digested **Li-AOIA@BF_4**.

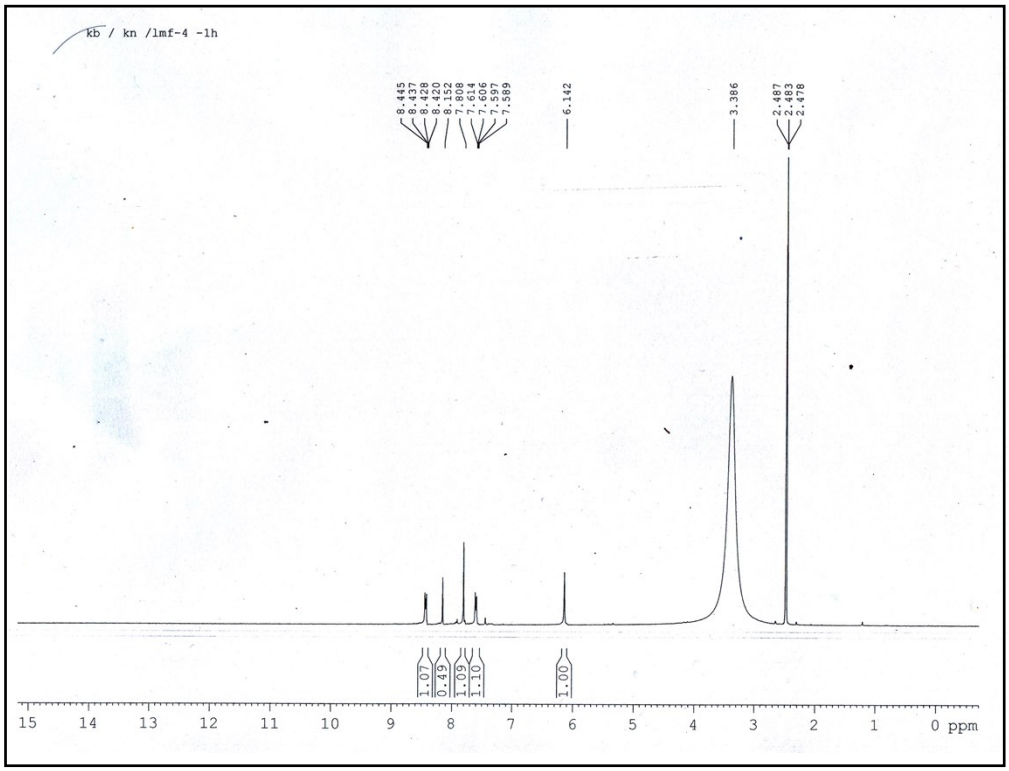

Fig. S22 [1]H NMR spectrum of digested **Li-AOIA@Cl**.

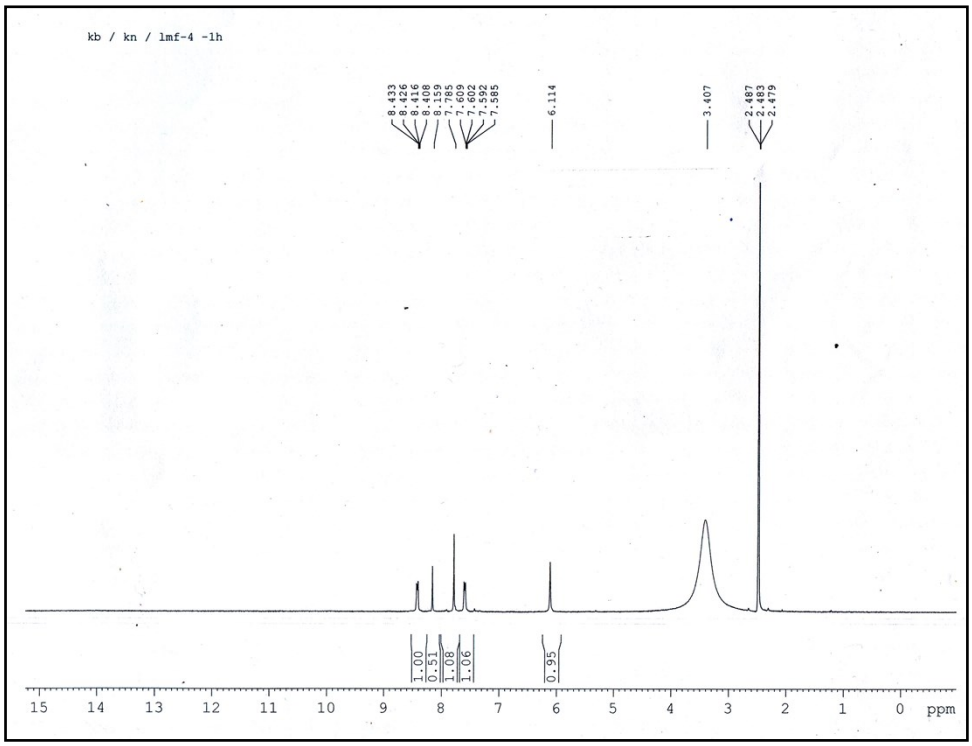

Fig. S23 [1]H NMR spectrum of digested **Li-AOIA@Br.**

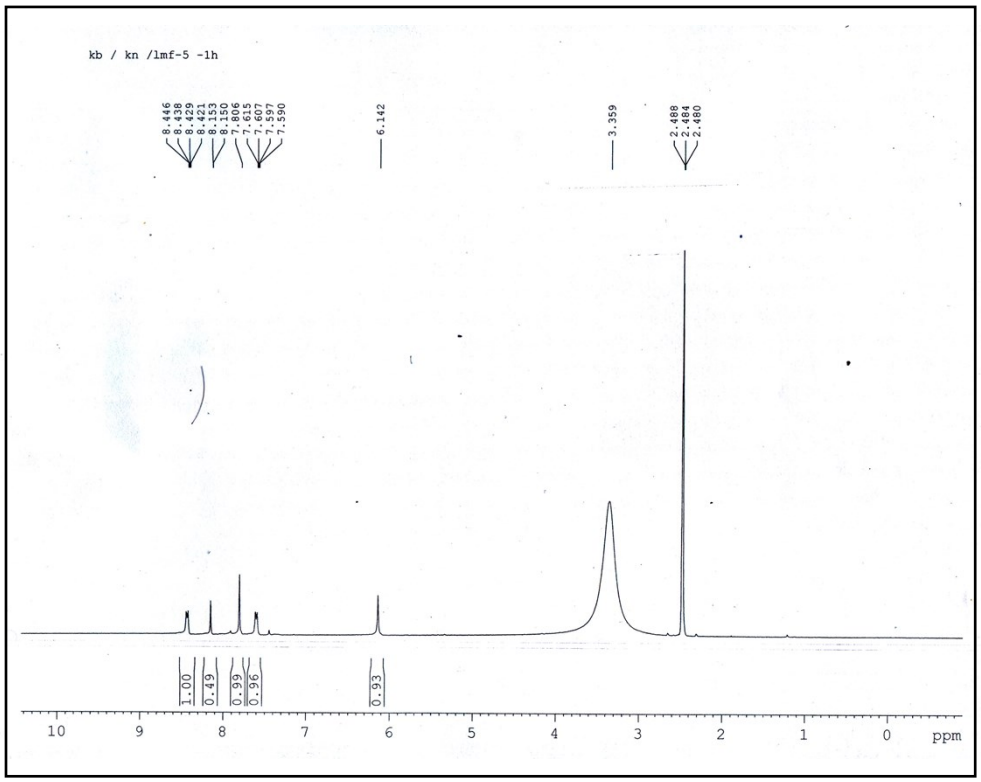

Fig. S24 [1]H NMR spectrum of digested **Li-AOIA@I.**

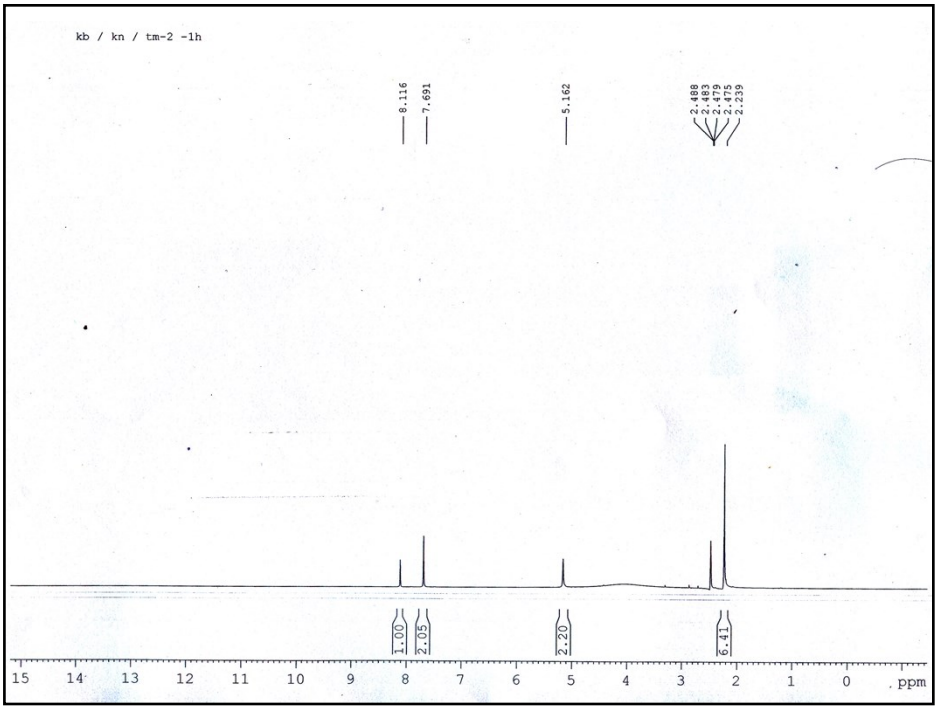

Fig. S25 ^{1}H NMR spectrum of digested **Li-TMCA@NO_3.**

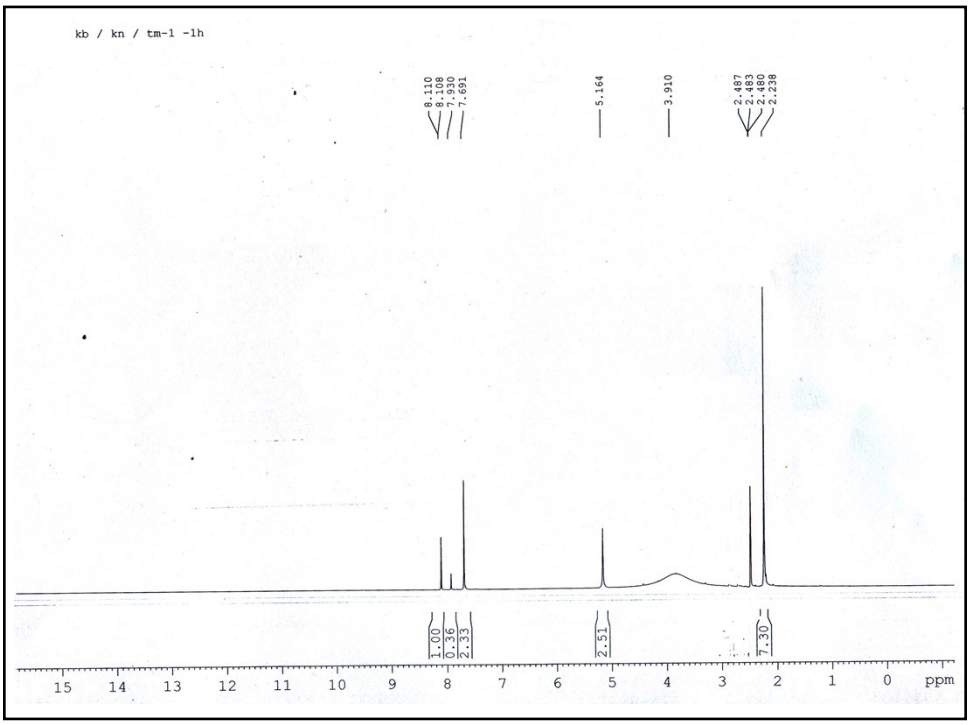

Fig. S26 ^{1}H NMR spectrum of digested **Li-TMCA@BF_4.**

Section S8: Electrical Conductivity Measurements

Impedance measurements were performed in a two electrode system by using a Hioki LCR meter over a frequency range of 10 Hz to 5 MHz. The pressed pellets were mounted on a metal block (Cu) and kept at 5×10^{-6} mbar vacuum pressure during measurements. For temperature dependent investigations, the temperature was controlled by a homemade temperature controller built around a PID unit (Honeywell DC1010). Temperature was recorded from a temperature sensor (Pt100) sitting next to the sample. The stability was better than ±0.5K throughout the whole temperature range. The ionic conductivity (σ) was calculated by using the low frequency end point of the semicircle as the resistance (R), area (A) and thickness (l) of the pellet based on $\sigma = l/(RA)$. The conductivity values were measured at different temperatures and by using Arrhenius equation of conductivity, the activation energy (E_a) was estimated from lnσ vs 1/T plot.

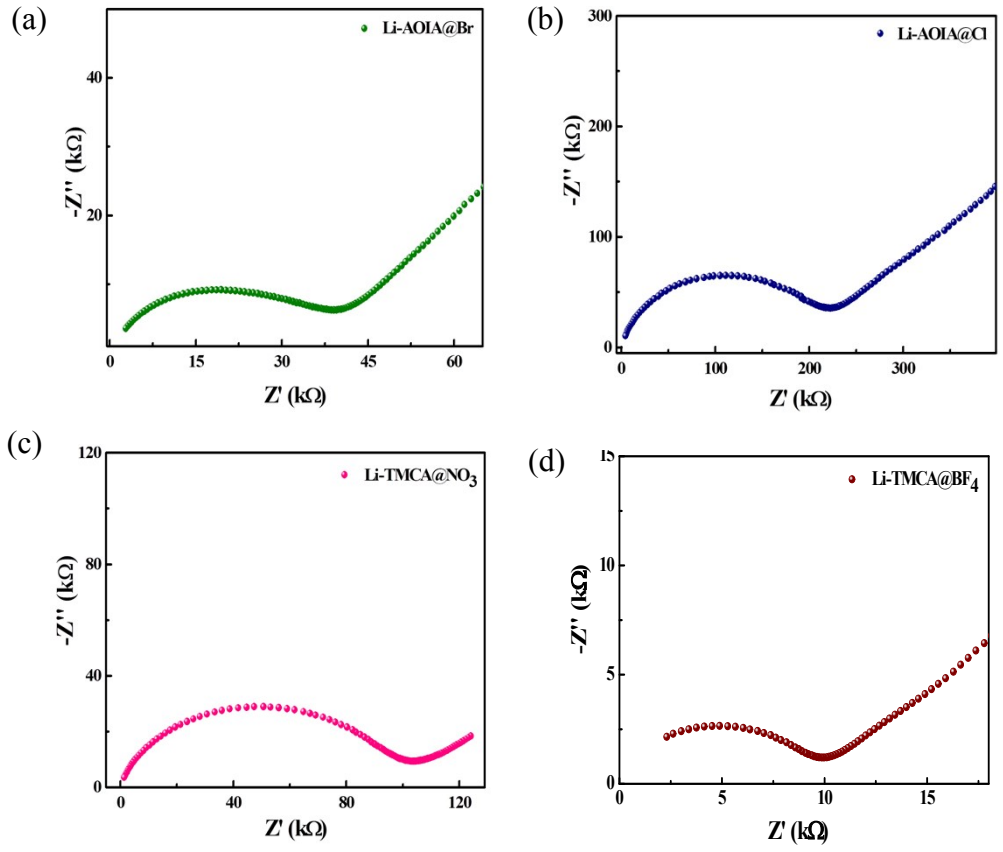

Fig. S27 Nyquist plots obtained from ac impedance measurement for (a) Li-AOIA@Br; (b) Li-AOIA@Cl; (c) Li-TMCA@NO_3 and (d) Li-TMCA@BF_4.

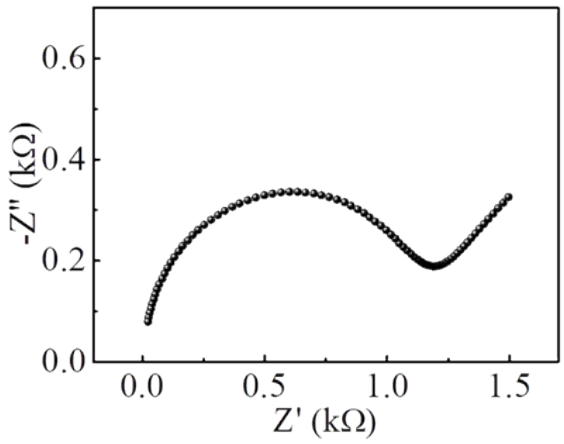

Fig. S28 Nyquist plots obtained from ac impedance measurement for LiOH treated MOF sample (**Li-AOIA@OH**).

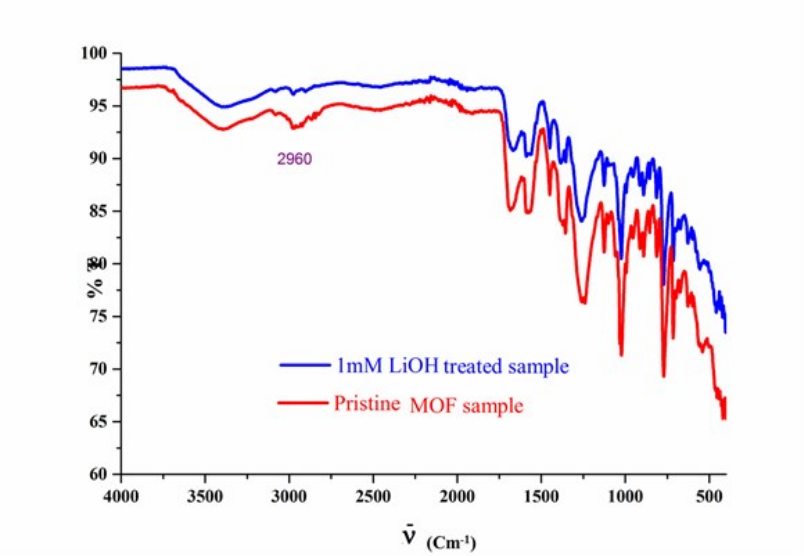

Fig. S29 FTIR spectra of **Li-AOIA** (red), and 1mM LiOH treated MOF sample **Li-AOIA@OH** (blue) indicating removal of the carboxylic acid proton.

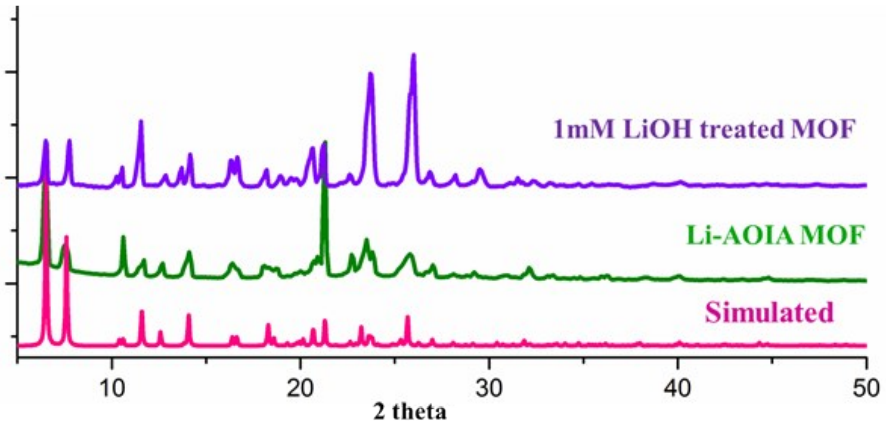

Fig. S30 PXRD patterns of **Li-AOIA** , and 1mM LiOH treated MOF sample.

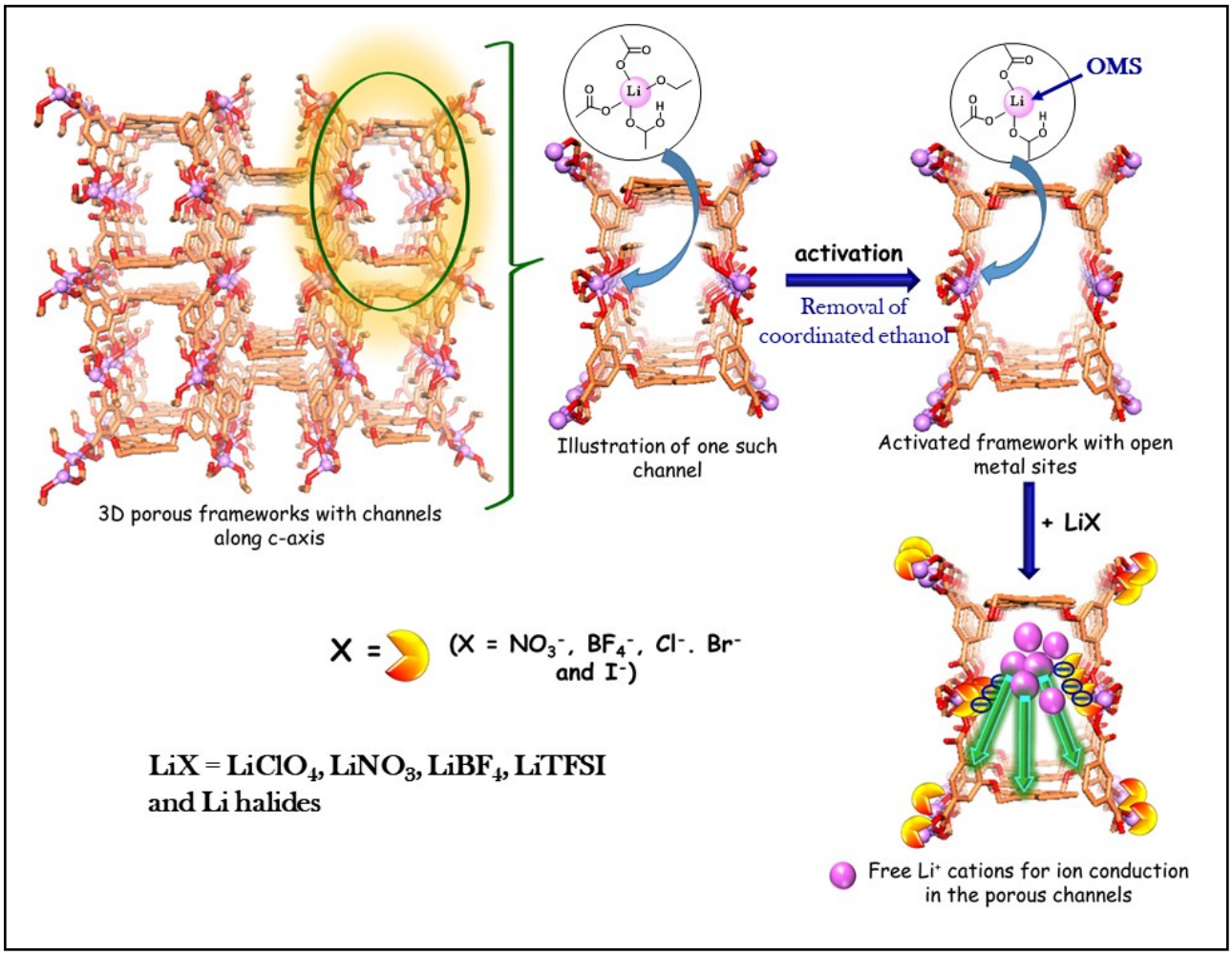

Scheme S1. Schematic representation of the porous ionic channels in **Li-AOIA**

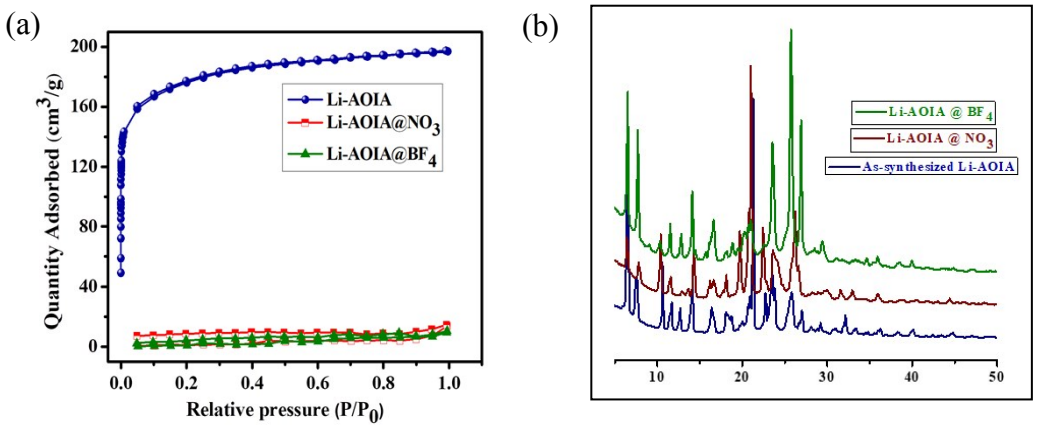

Fig. S31 (a) N_2 adsorption-desorption isotherms of **Li-AOIA** and the Li-doped MOFs (**Li-AOIA@NO_3** and **Li-AOIA@BF_4**); (b) experimental powder patterns of **Li-AOIA**, **Li-AOIA@NO_3** and **Li-AOIA@BF_4**.

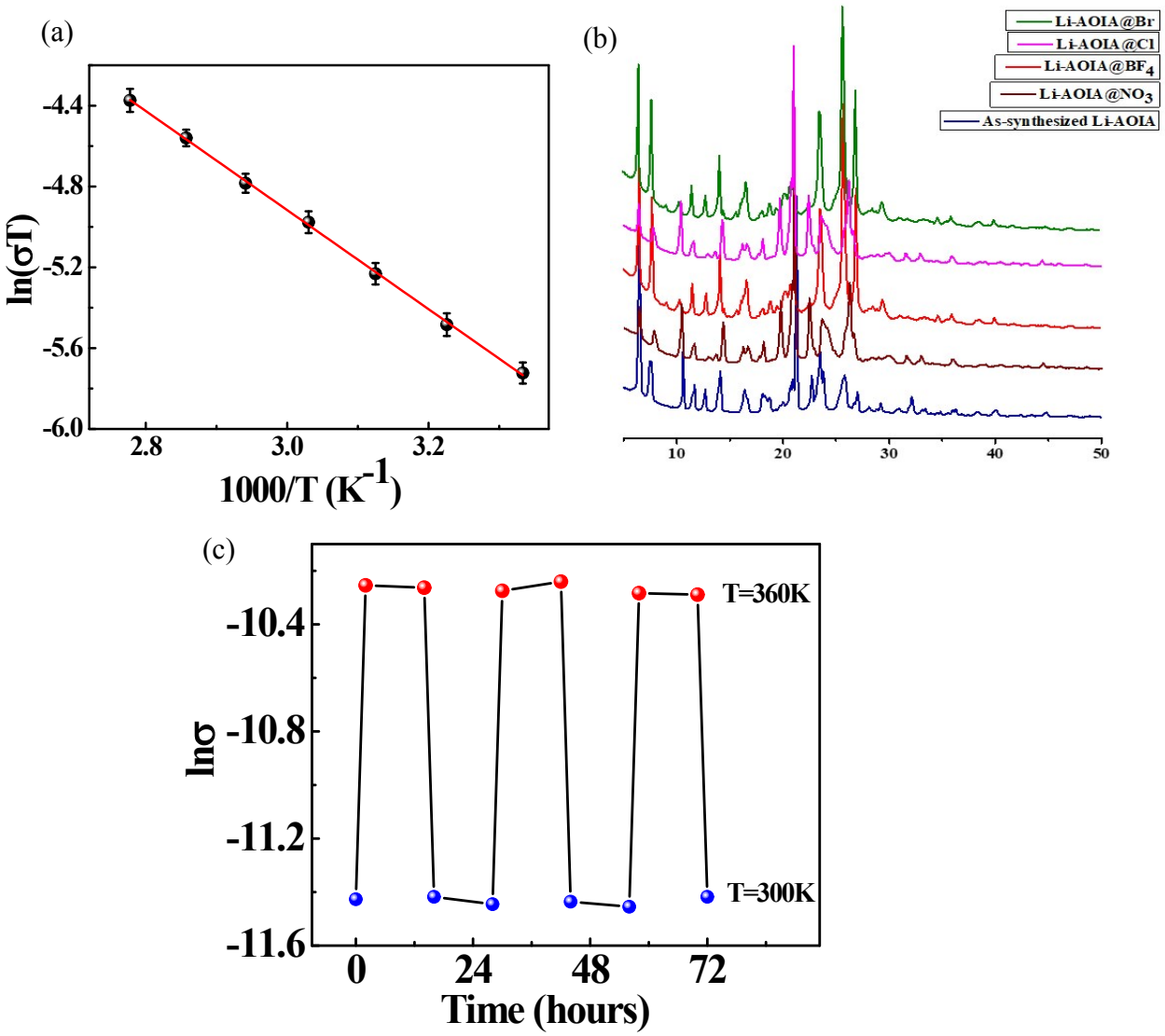

Fig. S32 (a) Variation of ln(σT) vs. 1000/K. The error bars were estimated from values obtained for identical samples (**Li-AOIA@BF_4**) in di□erent measurements; (b) Powder patterns of the solid-state electrolytes after ac impedance measurements; (c) Cycling performance of **Li-AOIA@BF_4**.

Section S9: Microscopic Analysis-FESEM, EDX and Elemental Mapping

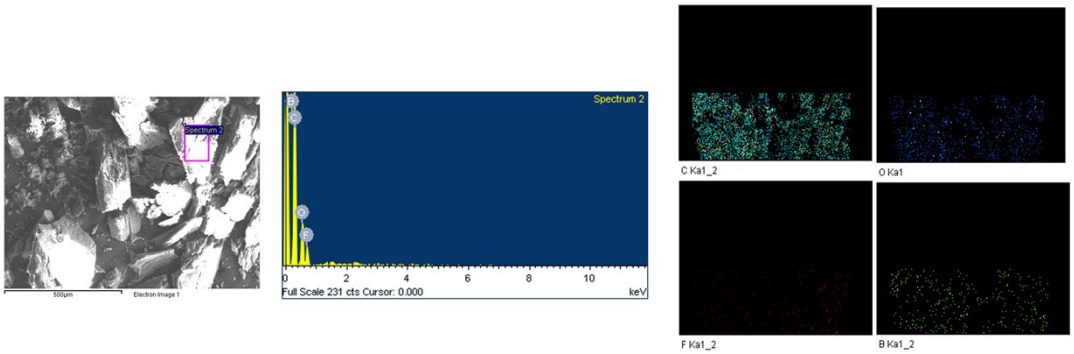

Fig. S33 FESEM, EDX and elemental mapping for **Li-AOIA@BF_4**

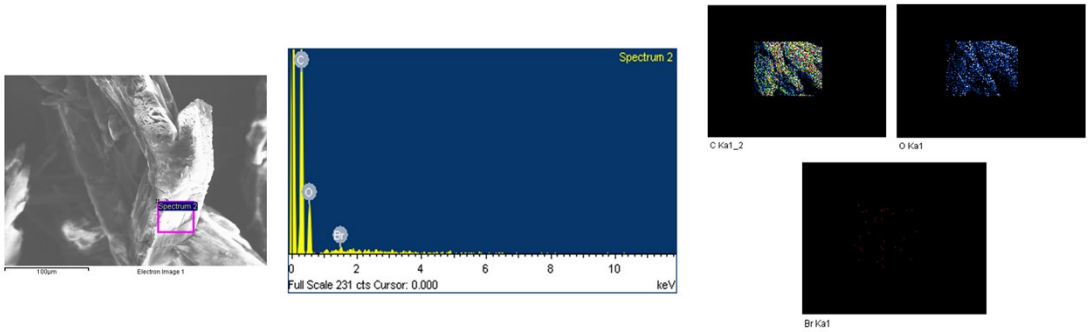

Fig. S34 FESEM, EDX and elemental mapping for **Li-AOIA@Br**.

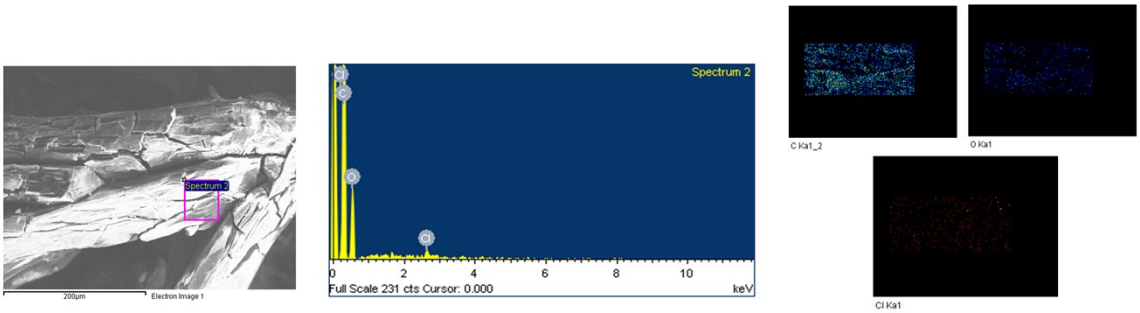

Fig. S35 FESEM, EDX and elemental mapping for **Li-AOIA@Cl**.

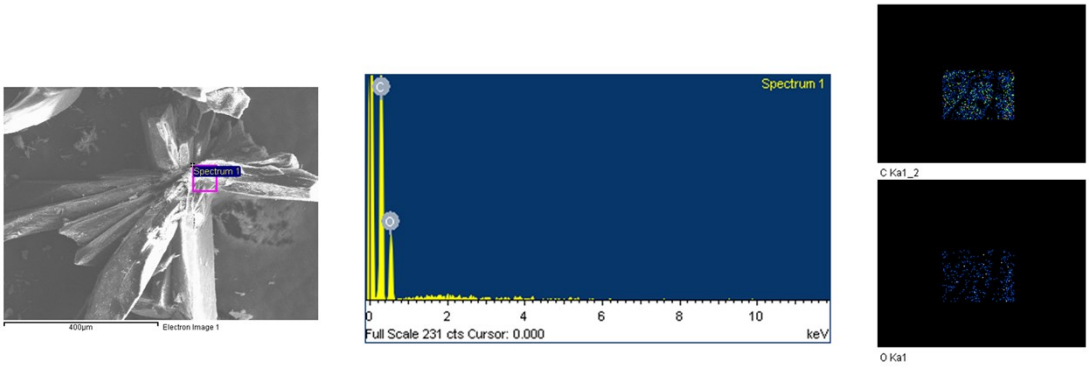

Fig. S36 FESEM, EDX and elemental mapping for **Li-AOIA@NO_3**.

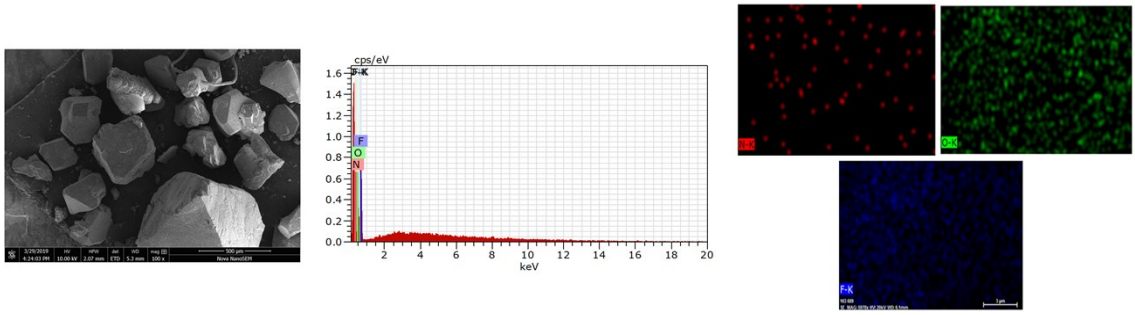

Fig. S37 FESEM, EDX and elemental mapping for **Li-TMCA@BF_4**

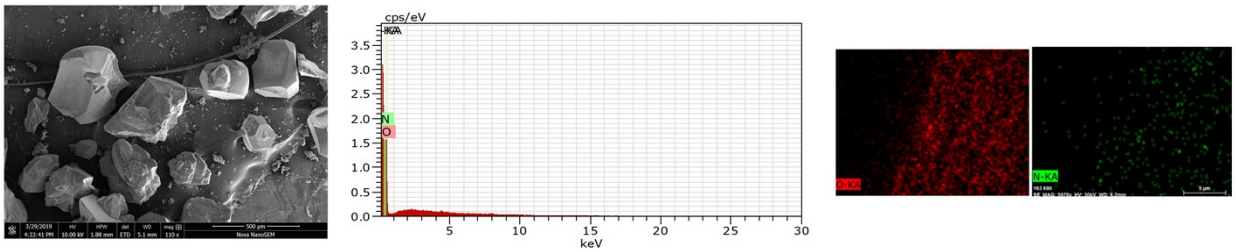

Fig. S38 FESEM, EDX and elemental mapping for **Li-TMCA@NO_3**

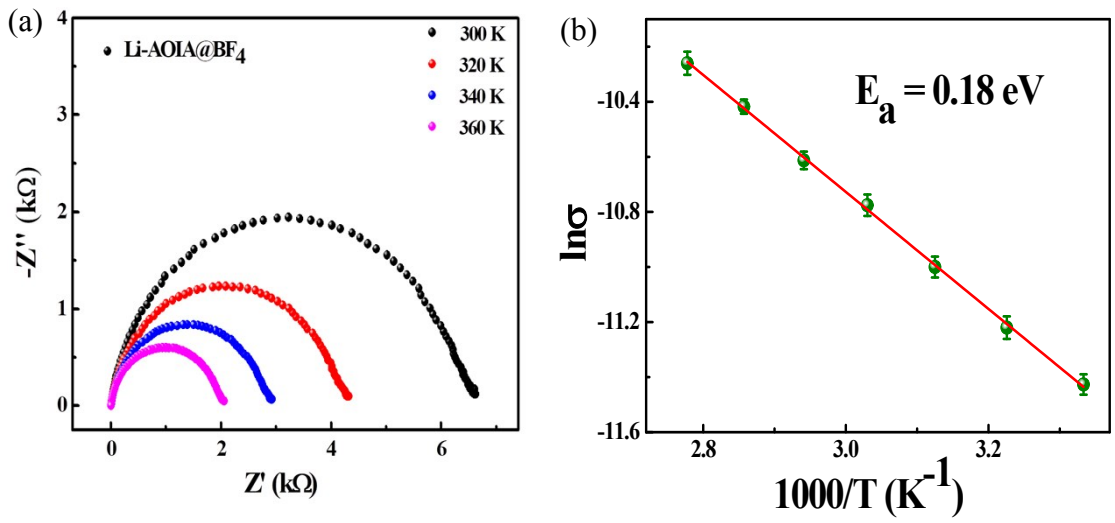

Fig. S39 (a) Nyquist plot for **Li-AOIA@BF_4** obtained from variable temperature ac impedance measurements; (b) Arrhenius plot and the corresponding activation energy of **Li-AOIA@BF_4**. The error bars were estimated from values obtained for identical samples in di□erent measurements.

Table S2: Comparison of surface area and hydrogen uptake capacity of reported Li-MOFs at 77K and 1 bar pressure.

Compounds (MOFs)	**BET Surface Area (m^2/g)**	**H_2 uptake (cm^3/g)**	**References**
$[Li_4(PyEP)_3(OH)]$	-	108.7	*Cryst. Growth Des*. **2016**, *16*, 6531−6536
CPM-46	592	-	*Cryst. Growth Des*. **2014,** *14*, 897−900
CPM-42	-	59.9	*Cryst. Growth Des.* **2015**, *15,* 2550−2554
$Li_4(OPy)_4$	440.3	108.7	*Chem. Commun.,* **2011**, *47*, 5536–5538
Li-AOIA	605	125	**This work**

Table S3: Results of ICP-AES analysis

Li-MOF@X electrolytes	**Amount of Li content after salt treatment**	**Conductivity (S/cm)**
Li-AOIA@NO_3	1.48%	5.53×10^{-6}
Li-AOIA@BF_4	1.52%	1.09×10^{-5}
Li-AOIA@Cl	1.32%	2.08×10^{-6}
Li-AOIA@Br	1.28%	3.42×10^{-6}
Li-TMCA@NO_3	0.82%	5.03×10^{-7}
Li-TMCA@BF_4	0.9%	2.93×10^{-6}

References:

S1. Zhou, L.-P.; Sun, Q.-F. A Self-assembled Pd_2L_4 Cage that Selectively Encapsulates Nitrate. *Chem. Commun*. **2015**, *51*, 16767-16770.

S2. Nath, K.; Bhunia, K.; Pradhan, D.; Biradha, K. MOF-Templated Cobalt Nanoparticles Embedded in Nitrogen-Doped Porous Carbon: A Bifunctional Electrocatalyst for Overall Water Splitting. *Nanoscale Adv.* **2019**, *1*, 2293–2302.

S3. Sheldrick, G. M. *SHELXL-2014*; University of Göttingen and Bruker AXS: Karlsruhe, Germany, 2014.